IEEE Access
Multidisciplinary | Rapid Review | Open Access Journal

Received November 23, 2019, accepted January 2, 2020, date of publication January 8, 2020, date of current version January 16, 2020.

Digital Object Identifier 10.1109/ACCESS.2020.2964780

Numerical Study of Voltage-Gated Ca^{2+} Transport Irradiated by Terahertz Electromagnetic Wave

WENFEI BO, LIANGHAO GUO, YANG YANG, JIALU MA, KAICHENG WANG, JINGCHAO TANG, ZHE WU, BAOQING ZENG, AND YUBIN GONG, (Member, IEEE)
School of Electronic Science and Engineering, University of Electronic Science and Technology of China, Chengdu 610054, China

Corresponding author: Yubin Gong (ybgong@uestc.edu.cn)

This work was supported by the National Natural Science Foundation of China under Grant 61921002.

ABSTRACT This paper simulates Ca^{2+} transmembrane transport through voltage-gated Ca^{2+} channels in response to terahertz electromagnetic irradiation. The active transport of Ca^{2+} ions is taken into considerations in the Ca^{2+} transport. Temperature variations due to terahertz electromagnetic loss in physiological medium are simulated. The electromagnetic interaction between terahertz fields and physiological mobile ions at the cellular level is deduced from relativistic electrodynamics. It shows that effects of $0.1 \sim 3$ THz electromagnetic fields on cell mobile ions are primarily due to effects of electric fields, and effects of magnetic fields at the cellular level are insignificant. In addition, numerical simulation reveals that terahertz irradiation causes vibration of membrane potential, which is able to activate voltage-gated Ca^{2+} channels. Besides, bioeffects of terahertz frequency, irradiation duration and electric intensity on the increment of intracellular Ca^{2+} concentration due to activation of voltage-gated Ca^{2+} channels are revealed. Meanwhile, numerical results show that temperature rises are inconsequential in the case of different irradiation parameters, indicating the non-thermal bioeffects of voltage-gated Ca^{2+} transmembrane transport due to terahertz irradiation. Furthermore, the results also reveal that thermal bioeffect can be significant if the irradiation duration is raised long enough for high-dose terahertz irradiation. The numerical simulations lay the basis for understanding the bioeffects of terahertz irradiation on Ca^{2+} transmembrane transport and pave the way for further exploration in modulation of intracellular Ca^{2+} concentration with terahertz electromagnetic wave.

INDEX TERMS Biological effects of electromagnetic radiation, modeling and simulations, calcium ions, voltage-gated calcium channel, active transport.

I. INTRODUCTION

As an exploring spectrum located between microwave and infrared region, terahertz (THz) electromagnetic field shows great potential applications in life sciences [1], [2].

Apart from terahertz biomedical imaging and terahertz detection for biomolecules and tissues in diseases [3]–[5], bioeffects of terahertz electromagnetic irradiation have caused an intense interest and attention in recent years [6], [7]. Along with the bioeffects, a high-dose THz irradiation is likely to produce significant thermal effects in biological cells or tissues [8], [9] as a result of the strong absorption of THz electromagnetic fields in water [10], [11]. And the THz bioeffects can be explained by the heat effect of the same amount of temperature increment [12].

In contrast, the bioeffects in the case of low-dose THz irradiation are unable to be explained by the heat effect, and the temperature increments along with these bioeffects are insignificant. In 2005, Ostrovskiy et. al. observed that THz irradiation improved the repairmen of localized burns [13]. In 2008, Kirichuk et. al. observed that both female and male rats with the exposure to THz irradiation showed complete recovery from platelet aggregation [14]. In the same year, Kirichuk and Androvov et. al. observed that THz-irradiated isokets showed more reduction of blood viscosity and increase of erythrocyte deformability in human blood of

The associate editor coordinating the review of this manuscript and approving it for publication was Pu-Kun Liu.

patients with unstable angina [15]. In 2009, Kirichuk et. al. observed that albino rats in response to THz irradiation exhibited an enhancement of platelet aggregation and increased levels of depression [16]. In 2011, Wilmink et al. showed the temperature increments along with those bioeffects were negligible by means of finite-difference time-domain modeling approach [6], [12]. Those indicate that THz electromagnetic irradiation is capable of modulating physiological activities and functions in a non-thermal way. However, the mechanism underneath the non-thermal bioeffects of THz irradiation is unknown.

Calcium ions are critical physiological ions. The transport of Ca^{2+} ions through plasma membrane is the basis for various physiological functions and processes in a stable temperature. It is of considerable significance to study the transmembrane transport of Ca^{2+} ions under terahertz irradiation in order to make clear the underlying mechanism of the terahertz bioeffects and guide further clinical applications, like therapies of cardiovascular diseases etc.

The non-thermal increase in intracellular Ca^{2+} concentration in neuroblastoma cells is observed, and the phospholipid bilayer membrane electroporation for ion transport is simulated with molecular dynamics simulations under the radiation of picosecond electric pulse, whose fast rise edge contains signal component in terahertz frequency [17]. Although the applied picosecond electric pulse [17] contains a few amounts of energy in terahertz spectral region, the pulse is a broadband signal which also contains much more energy in low frequency region from megahertz to kilohertz frequency, including direct current. Furthermore, it is known that the electric pulse containing the low frequency region, for example, unipolar or bipolar nanosecond electric pulse, opens pathways in the plasma membrane for the entry of extracellular Ca^{2+} ions [18]–[20]. Additionally, molecular dynamics simulations show that the electropore formation for the entry of extracellular Ca^{2+} ions by the applied picosecond pulse is similar to that by nanosecond electric pulse [17]. Therefore, it is uncertain to attribute the entry of Ca^{2+} ions to terahertz component, low frequency component or both.

In addition, the impacts of terahertz sinusoidal wave and a train of unipolar pulses with terahertz repetition frequency on electropore formation are compared with molecular dynamics simulations [21]. The simulations show that the train pulses with THz repetition frequency, which contain a significant amount of low frequency component and some amount of THz frequency component, leads to the electroporation in phospholipid bilayer membrane, and that the THz sinusoidal wave, which contain only THz frequency component without the low frequency component [22], fail to induce the electroporation [21]. Besides, it is observed that the effect of THz irradiation on the entry of propidium, which is a kind of impermeable dye to intact plasma membrane in healthy cells, is dependent on the dose of the irradiation [23]. And for the occurrence of the entry of propidium, the bioeffect is no more non-thermal with the induced temperature rise of as high as 6° [23].

In contrast to possible electroporation in response to terahertz irradiation, voltage-gated Ca^{2+} channels (VGCCs) embedded in phospholipid bilayer membrane are primary physiological channels responsible for Ca^{2+} transmembrane transport in excitable cells. Those channels link the electric signals and nonelectrical physiological processes, and play crucial roles in physiological processes like the regulation of heart beat etc. However, the influence of terahertz irradiation on voltage-gated (VG) Ca^{2+} flux remains unknown.

In this paper, transmembrane transport of Ca^{2+} ions through VGCCs is numerically studied under the irradiation of terahertz electromagnetic waves. The applied terahertz waves are narrow-banded signals, which are achieved with a terahertz continuous sinusoidal electromagnetic wave with a limited irradiation duration. Firstly, an electromagnetic response model at cellular level is proposed on the basis of relativistic electrodynamics to analytically study the electric and magnetic fields within the cell as well as the electromagnetic interactions between the THz fields and cell mobile ions, which are depicted in detail in Section II. Then, the transmembrane transport of Ca^{2+} ions through VGCCs in response to THz irradiation is simulated with the consideration of active transport. Temperature change due to THz irradiation is taken into considerations based on Debye relaxation theory and thermodynamic principles. The modeling details and simulation methods are described in Section III. In Section IV, numerical results are presented and discussed. And Section V summarizes the conclusions.

II. DERIVATION OF ELECTROMAGNETIC INTERACTION BETWEEN THz FIELDS AND PHYSIOLOGICAL IONS

Under terahertz irradiation, the fields in the cell region are composed of the fields due to the physiological ions and the fields of the irradiated THz electromagnetic wave.

A. FIELDS DUE TO MOBILE PHYSIOLOGICAL IONS IN THE CELL REGION

The electric field excited by a static physiological ion in intracellular or extracellular medium at time t can be obtained by Gauss's law,

$$E_1(r,t) = q_1 / \left[4\pi\varepsilon_0\varepsilon_r r^2(t)\right] \tag{1}$$

where q_1 is charge quantity of the ion, ε_r is the relative permittivity of the medium, ε_0 is the permittivity in vacuum, and $r(t)$ is the spatial position of the observer relative to the position of the ion at time t.

And the static ion excites no magnetic field,

$$H_1(r,t) = 0 \tag{2}$$

When it moves in intracellular or extracellular medium, the physiological ion excites not only electric field but also magnetic field. According to the covariance in relativity, the electric field excited by the mobile physiological ion is the Lorentz transformation of (1) and (2), as is

given by,

$$E_1(r,t) = q_1 \cdot \left[1 - v^2(t)/c^2\right] \Big/ \left\{4\pi\varepsilon_0\varepsilon_r r^2(t)\left[1 - v^2(t)\sin^2\langle\vec{r}(t), \vec{v}(t)\rangle/c^2\right]^{3/2}\right\} \quad (3)$$

where c is the speed of light, $v(t)$ is the speed of the ion at t, and $\langle\vec{r}(t), \vec{v}(t)\rangle$ is the angle between the directions of the displacement r and the velocity v at t.

Likewise, the magnetic field excited by the ion can be obtained from the Lorentz transformation of (1) and (2) as,

$$H_1(r,t) = q_1 v(t)\left[1 - v^2(t)/c^2\right]\sin\langle\vec{r}(t), \vec{v}(t)\rangle \Big/ \left\{4\pi\varepsilon_0\varepsilon_r\mu_0 c^2 r^2(t)\left[1 - v^2(t)\sin^2\langle\vec{r}(t), \vec{v}(t)\rangle/c^2\right]^{3/2}\right\} \quad (4)$$

At room temperature 297.15K, the most probable speeds of physiological calcium, sodium, potassium and chloride ions are 351.0, 463.5, 355.4 and 373.3 m/s respectively in the medium. Since the speeds of the ions are far smaller than the speed of light, $v(t)/c$ approaches 0. In this case, (3) reduces to (1), and (4) reduces to the Biot-Savart law.

As a result, there is no coupling between the electric and magnetic fields excited by mobile physiological ions, although the electric and magnetic fields vary with time because of the change in ion spatial distribution with time.

B. FIELDS DUE TO TERAHERTZ ELECTROMAGNETIC IRRADIATION

Since any field waveform can be expressed by a sum of a series of sinusoidal waveforms, it is assumed that the applied electromagnetic wave is of a sinusoidal form. As shown in Fig. 1, the electromagnetic wave propagates in the direction of X axis. Thus, the electric field is given by,

$$E_2(r,t) = E_0 \exp\left[i2\pi\left(ft - x\sqrt{\varepsilon_r}/\lambda_0\right)\right] \quad (5)$$

where f is frequency of the irradiated THz electromagnetic field, λ_0 is the wavelength in vacuum, i is the imaginary unit, E_0 is the amplitude of the field, and r is the spatial position of the observer with abscissa x and ordinate y.

From (5), the ratio of the electric field $E_2(r_{C6}, t)$ at C6 to $E_2(r_{C12}, t)$ at C12 is expressed as,

$$E_2(r_{C6},t)/E_2(r_{C12},t) = \exp\left[-i2\pi\left(x_{C6} - x_{C12}\right)\sqrt{\varepsilon_r}/\lambda_0\right] \quad (6)$$

where x_{C6} and x_{C12} are respectively abscissa values at C6 and C12 from Fig. 1.

In (6), $(x_{C6} - x_{C12})$ is the diameter of the cell 6.6 μm. In the spectrum range from 0.1 to 3THz, the vacuum wavelength λ_0 is at the range from 0.1 to 3 mm. The relative permittivity ε_r in intracellular and extracellular media is lower than 3.6 from 1 to 3THz, lower than 6 from 0.3 to 1THz, lower than 6.74 at 0.2THz, and lower than 12.36 at 0.1THz [24]. In this case, $(x_{C6} - x_{C12})\sqrt{\varepsilon_r} \ll \lambda_0$, and then the right side in (6) tends to 1. Therefore, the electric field of the irradiated THz fields at C12 is nearly identical to that at C6 at any time t, and there is few phase difference of the fields between C6 and C12. Since the distance between C6 and C12 is the farthest in the cell in the propagation direction of the wave, it means that the electric fields of the THz electromagnetic wave synchronously vary within the cell without phase difference at any time t. Then, it follows that the electric field of the THz electromagnetic irradiation is approximately uniform spatially in the cell region.

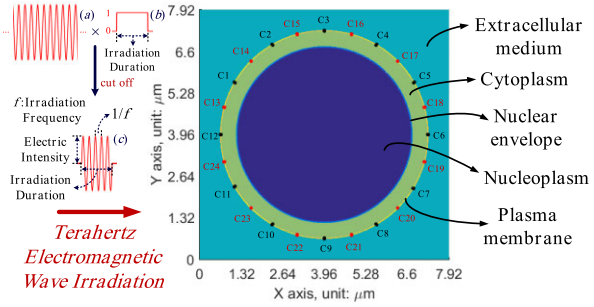

FIGURE 1. Schematic illustration of THz electromagnetic irradiation on a NG108-15 cell. In (c), an illustration of irradiated THz electromagnetic wave in time domain as well as the descriptions of electromagnetic parameters is depicted. The irradiated wave in (c) is derived from a continuous sinusoidal electromagnetic wave in (a) that is cut off to produce the limited irradiation duration in (b). The wave propagates along x-axis, and its electric field is along y-axis. C1, C2, ..., C12 are voltage-gated calcium channels, and C13, C14, ..., C24 are active transport channels for calcium ions.

Because of the spatial uniformity of electric field in the cell region, the spatial variation of electric field is zero at any time t. Then, it follows that,

$$\nabla \times \vec{E}_2(r,t) = 0 \quad (7)$$

Based on Maxwell equations, it can be deduced that,

$$\partial\vec{H}_2(r,t)/\partial t = -\nabla \times \vec{E}_2(r,t)/\mu_0 = 0 \quad (8)$$

so the magnetic field $H_2(r, t)$ of the THz electromagnetic wave can be viewed as time invariant in the cell region.

C. DIELECTRIC RESPONSE OF CELL TO THE FIELDS

As the electric fields excited by mobile physiological ions at any time t are static in the cell region, the dielectric response to ion electric fields is static response at any t.

In contrast, the dielectric response to the electric fields of THz electromagnetic wave is frequency-dependent response. Because most of constituents are water in intracellular and extracellular media, the frequency-dependent dielectric response can be described by double Debye relaxation theory [25]. The double Debye relaxation theory is given by,

$$\hat{\varepsilon}(f) = \varepsilon_\infty + (\varepsilon_s - \varepsilon_2)/(1 + i2\pi f\tau_1) + (\varepsilon_2 - \varepsilon_\infty)/(1 + i2\pi f\tau_2) \quad (9)$$

TABLE 1. Parameter values for biological cells and extracellular medium in double Debye relaxation theory.

Symbol	Parameter Values for Biological Cell	Parameter Values for Extracellular Medium
ε_∞	3.4	1.7
ε_s	2.5	78.8
ε_2	23.8	3.6
τ_1	410.8 ps	8.0 ps
τ_2	1.8 ps	0.1 ps

where ε_∞ is the real part of the relative permittivity at the high frequency limit, ε_s is the static relative permittivity, ε_2 is the intermediate value of the real part of the relative permittivity, τ_1 and τ_2 are respectively the relaxation times relating to the first and second relaxation process.

The parameter values for biological cells and extracellular medium in the double Debye relaxation theory are measured with THz transmission time spectroscopy [24], which are listed in Table 1.

D. EFFECTS OF THE FIELDS ON MOBILE PHYSIOLOGICAL IONS IN CELL REGION

Since the speeds of mobile ions are far lower than the speed of light, the force from electromagnetic fields on the ions is classical Lorentz force. The force from electromagnetic fields is derived from electric and magnetic fields due to ions and irradiated THz wave.

From Section II. A, the electric and magnetic fields due to mobile ions are static and steady in the medium at any time t. Suppose that an arbitrary physiological ion q_1 has a relative velocity $v(t)$ compared with another arbitrary physiological ion q_2 in the medium of relative permittivity ε_r. Then the electric force $F_{ion-E}(r, t)$ and magnetic force $F_{ion-M}(r, t)$ on ion q_1 due to ion q_2 are respectively,

$$F_{ion\_E}(r,t) = q_1 q_2 / \left[4\pi\varepsilon_0\varepsilon_r r^2(t)\right] \tag{10}$$

$$F_{ion\_M}(r,t) = q_1 q_2 v^2(t) \sin^2\langle \vec{r}(t), \vec{v}(t)\rangle / \left[4\pi\varepsilon_0\varepsilon_r c^2 r^2(t)\right] \tag{11}$$

The ratio of magnetic and electric forces is,

$$F_{ion\_M}(r,t) / F_{ion\_E}(r,t) = v^2(t)\sin^2\langle \vec{r}(t), \vec{v}(t)\rangle / c^2 \tag{12}$$

Since $v^2(t)\sin^2\langle \vec{r}(t), \vec{v}(t)\rangle \ll c^2$, then $F_{ion-M}(r, t) \ll F_{ion\_E}(r, t)$. As a result, the force on a mobile ion due to other ions is dominated by electric force, and magnetic force is so small that it can be neglected.

Besides, in the case of irradiated THz electromagnetic fields, the electric force F_{EM-E} and magnetic force F_{EM-M} on q_1 are

$$F_{EM\_E}(r,t) = q_1 E_2(r,t) \tag{13}$$

$$F_{EM\_M}(r,t) = q_1\mu_0 v(t) H_2(r,t) \sin\left\langle \vec{v}(t), \vec{H}_2(r,t)\right\rangle \tag{14}$$

where $H_2(r, t)$ is the magnetic field of the THz electromagnetic wave at position r and time t, and μ_0 is permeability in vacuum.

For transverse electromagnetic plane wave, the ratio of electric and magnetic fields in intracellular or extracellular medium is given by,

$$E_2(r,t)/H_2(r,t) = \sqrt{\mu_0 / \left[\varepsilon_0\varepsilon_p'(f) - i\varepsilon_0\varepsilon_p''(f)\right]} \tag{15}$$

where p denotes the intracellular or extracellular medium. $\varepsilon_p'(f)$ and $\varepsilon_p''(f)$ are the real and imaginary parts of relative permittivity $\varepsilon_p(f)$ at the frequency f, respectively.

By dividing (14) by (13) and rearranging equations with (15), we obtain the ratio of magnetic and electric forces from THz electromagnetic wave on q_1,

$$F_{EM\_M}(r,t)/F_{EM\_E}(r,t) = v(t)\sqrt{\varepsilon_p'(f) - i\varepsilon_p''(f)}\sin\left\langle \vec{v}(t), \vec{H}_2(r,t)\right\rangle / c \tag{16}$$

where the speed of light in vacuum $c = 1/\sqrt{\varepsilon_0\mu_0}$, which is five to six orders of magnitude larger than $v(t)$. $\left|\sin\left\langle \vec{v}(t), \vec{H}_2(r,t)\right\rangle\right| \le 1$. And according to Section II. C, $\varepsilon_p'(f)$ and $\varepsilon_p''(f)$ are of the order of magnitude of -1 to 1 in the frequency range from 0.1 to 3THz. Hence, the right side in (16) is far smaller than 1, and then the magnetic force on the ion is much smaller than the electric force.

As a consequence, effects of magnetic fields due to mobile physiological ions and THz electromagnetic wave can be both ignored in the simulation of cell ion transport in response to $0.1 \sim 3$ THz electromagnetic irradiation.

III. Ca^{2+} TRANSMEMBRANE TRANSPORT MODEL AND SIMULATION METHODS

A. THERMAL ANALYSIS OF THz ELECTROMAGNETIC IRRADIATION

Temperature variations due to absorption loss of THz electromagnetic wave in physiological media are taken into considerations in the study of Ca^{2+} transmembrane transport through VGCCs. In view of periodic arrangement, cells at the vicinity of the cell of interest are identically exposed to the THz electromagnetic wave. Besides, the irradiation duration is short. Therefore, the cell system in Fig. 1 can be considered as an adiabatic system.

Given the fact that cell is not a magnetic medium, electric work due to the THz electromagnetic irradiation exclusively causes the change in internal energy of the system. The change in internal energy of part p is given by,

$$\partial U_p(t)/\partial t = P_{e\_p}(t) + k_{ther} Vol_p \nabla^2 T_p(t) \tag{17}$$

where $U_p(t)$ is the internal energy in part p of the system at time t, P_{e_p} the electrical power on part p, k_{ther} the thermal conductivity, Vol_p the volume of part p, $T_p(t)$ the temperature in part p at t, $k_{ther} Vol_p \nabla^2 T_p(t)$ the heat transfer with the other part in the system at t. Owing to adiabatic system, the heat transaction between the system and the surroundings is zero,

that is, $dT|_{boundary} = 0$. The initial temperature $T|_{t=0} = 297.15$K.

The electric field is of the form (5), and then the electrical power on the system can be deduced from energy balance equation for electromagnetic waves [26] by,

$$P_{e\_p} = \left[\sigma_p/(2\pi f) + \varepsilon_0\varepsilon_p''(f)\right]\pi Vol_p f E_0^2 \tag{18}$$

where σ_p is the conductivity in part p.

The change in internal energy is relevant to the change in temperature,

$$\partial U_p(t)/\partial t = c_{SHC} \cdot m_p \cdot \partial T_p(t)/\partial t \tag{19}$$

where c_{SHC} is specific heat capacity and m_p is the mass in part p.

The conductivity in intracellular or extracellular medium σ_p is on the order of magnitude of -1 to 0 [27]. Then, $\sigma_p/(2\pi f) \ll \varepsilon_0\varepsilon_p''(f)$ in the frequency range from 0.1 to 3THz. Thus, joule loss can be ignored and the electrical power in (18) only results from electric polarization loss. In this case, by neglecting joule loss and rearranging (17), (18) and (19), the temperature variation with time in part p of the system is,

$$\partial T_p(t)/\partial t = \left[\pi f \varepsilon_0 \varepsilon''(f) E_0^2 + k_{ther}\nabla^2 T_p(t)\right]/(c_{SHC}\rho) \tag{20}$$

where ρ is the mass density.

B. MODEL OF Ca^{2+} TRANSMEMBRANE TRANSPORT THROUGH PHYSIOLOGICAL CHANNELS WITH EXPOSURE TO THz ELECTROMAGNETIC WAVE

As shown in Fig. 1, VGCCs are simulated by twelve model channels C1, C2, …, and C12, which are uniformly distributed in the plasma membrane. Each of the model channels is responsible for one twelfth of whole-cell VG Ca^{2+} flux. The whole-cell VG Ca^{2+} flux is derived on the basis of facilitated diffusion model [28], and the model parameters are determined by electrophysiological experimental data of NG108-15 cells [29], [30]. Similarly, active transport of calcium ions through plasma membrane is modeled by uniformly distributed C13, C14, …and C24, each of which is responsible for one twelfth of whole-cell active transport calcium flux. The whole-cell active transport flux is deduced from the active transport model [31] and experimental data in NG108-15 cells [32]. The electrodiffusion of calcium ions is simulated in intracellular and extracellular media based on Nernst-Planck equation [33]. The corresponding modeling details are concretely presented in our earlier work [19].

C. SIMULATION METHODS

The physiological membrane potential (MP) of the cell is simulated by evaluating the electric field profile of mobile physiological ions in the cell region. The electric field profile is estimated by finite difference method (FDM). The Ca^{2+} fluxes with time in intracellular and extracellular media as well as Ca^{2+} transmembrane transport are simulated with particle-in-cell simulation method (PIC-SM). The details of

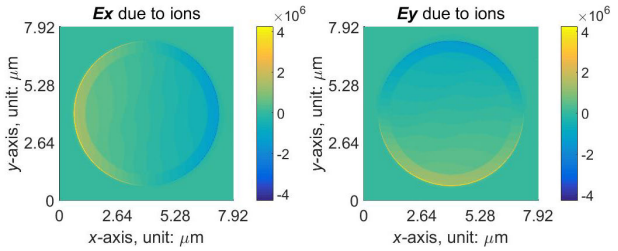

FIGURE 2. Electric field profiles due to physiological ions in the cell region under resting conditions. The intensity values of the electric field are depicted based on the color bar in V/m. (a) x-component of electric field due to ions. The positive value denotes the direction of the field in $+x$-axis while the negative value indicates the direction along $-x$-axis, (b) y-component of electric field due to ions. The positive value denotes the direction of the field in $+y$-axis, while the negative value indicates the direction along $-y$-axis.

FDM for the evaluation of electric field profile and PIC-SM are specifically described in [19]. Temperature profile in the cell region at each discretized time point t_n is estimated by (20), where the subscript n denotes iteration index. THz time-harmonic electric fields are added into the electric field profile due to ions according to superposition principle of electric field.

IV. NUMERICAL RESULTS AND DISCUSSIONS

As shown in Fig. 1, the irradiated THz electromagnetic wave propagates along $+x$-axis and its electric field fluctuates along y-axis. The NG108-15 cell is under resting conditions before the THz irradiation.

A. SIMULATION OF BIOLOGICAL CELL UNDER PHYSIOLOGICAL RESTING CONDITIONS

Fig. 2 shows the electric field profile due to ions in the inside and outside of the cell under physiological resting conditions. In comparison of Fig. 1 and Fig. 2, it can be seen that both x- and y-components of the electric field are mainly distributed on the plasma membrane. This is because the imbalance of ion concentrations between intracellular and extracellular media induces an electric potential difference across the plasma membrane, which is referred to as physiological membrane potential.

The simulated MP is around -60 mV, which is basically in agreement with the experimental measurements in NG108-15 cells [29], [30]. Besides, the electric field is almost zero in the extracellular medium far from the cell, which is consistent with the electric neutrality of the medium.

B. IRRADIATION OF LOW-DOSE TERAHERTZ ELECTROMAGNETIC WAVE

Fig. 3 shows the MPs at VGCCs within 8ns under the irradiation of a 1-THz, 15-kV/cm, 500-ps electromagnetic wave. During the irradiation, it can be seen that MPs vibrate due to the vibration of electric field of THz electromagnetic wave. During the vibration, MP exceeds the activation

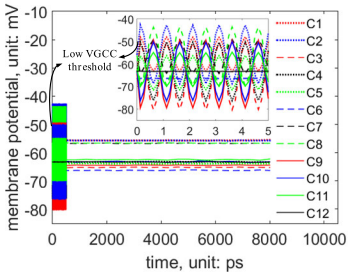

FIGURE 3. Membrane potentials (MPs) with respect to time at VGCC C1, C2, ..., C12 within 8ns under the irradiation of THz electromagnetic wave of 1-THz frequency, 15-kV/cm intensity, 500-ps duration. THz electromagnetic wave is applied at 0 ps. Threshold potential -50 mV for the activation of low VGCCs is marked. The inset in the figure zooms in on time to show representative vibrations of MPs during irradiation.

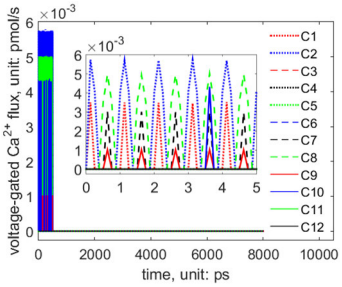

FIGURE 4. Voltage-gated (VG) calcium fluxes in terms of time at C1, C2, ..., C12 within 8ns under the irradiation of THz electromagnetic wave of 1-THz frequency, 15 kV/cm-intensity, 500-ps duration. THz electromagnetic wave is applied at 0 ps. The inset zooms in on time to show representative VG Ca^{2+} fluxes during irradiation.

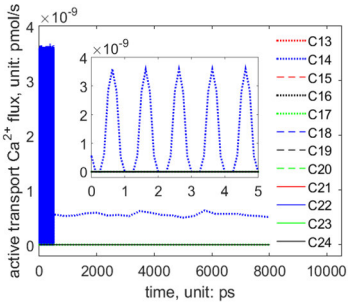

FIGURE 5. Active transport calcium fluxes in terms of time at C13, C14, ..., C24 within 8ns under the irradiation of THz electromagnetic wave of 1-THz frequency, 15-kV/cm intensity, 500-ps duration. THz electromagnetic wave is applied at 0 ps. The inset zooms in on time to show representative active transport Ca^{2+} fluxes during irradiation.

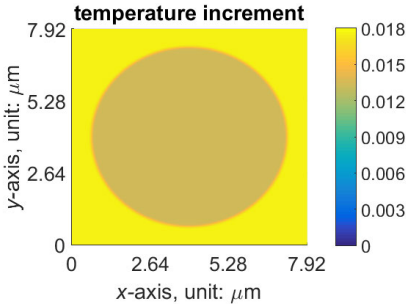

FIGURE 6. Temperature rise from initial temperature 297.15K in the cell region at 8ns with the exposure to THz electromagnetic wave of 1-THz frequency, 15-kV/cm intensity, 500-ps duration. The values of the temperature increment are depicted with the color bar in K.

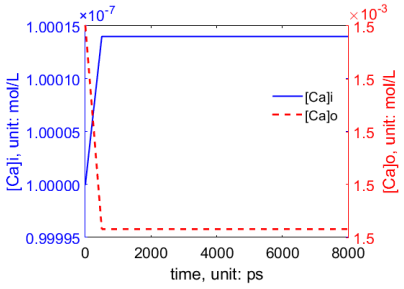

FIGURE 7. Variations of Ca^{2+} concentration due to the activation of VGCC with respect to time within 8ns in response to the irradiation of THz electromagnetic wave of 1-THz frequency, 15-kV/cm intensity, 500-ps duration. [Ca]i and [Ca]o respectively denote intracellular and extracellular Ca^{2+} concentration.

threshold -50mV of low VGCCs [29], [30], and opens the VGCCs to allow Ca^{2+} ions to go through. This is consistent with a series of physical models of VGCC, in which the gate of VGCC is as a consequence of the electrostatic energy barrier across the membrane [34], [35]. When the MP is below the activation threshold, the electrostatic field in the through hole of VGCC provides an energy barrier for extracellular Ca^{2+} ions to go through. And when the potential exceeds the threshold, the electrostatic energy profile changes to cancel the barrier and VGCC is open to extracellular Ca^{2+} ions for going through instead.

After the exposure to the THz electromagnetic wave, MPs stop vibration and restore to initial resting potential (see Fig. 3). And VGCCs close accordingly after the exposure. Fig. 4 presents the VG calcium fluxes in response to the THz electromagnetic irradiation. During the irradiation, extracellular calcium ions flow into the cell through VGCCs. After the irradiation, VG calcium fluxes become zero due to the closing of the channels. Fig. 5 illustrates the active transport Ca^{2+} effluxes in response to the THz wave. In comparison of Fig. 4 and 5, it is obvious that the active transport calcium effluxes are six orders of magnitude smaller than the VG calcium influxes. In this case, the effect of active transport of Ca^{2+} ions can be overlooked.

From Fig. 6, the maximum temperature rise is as small as 0.018 K, which indicates the non-thermal characteristics of VG Ca^{2+} influxes in response to the 1-THz, 15-kV/cm, 500-ps electromagnetic irradiation.

As illustrated in Fig. 7, intracellular Ca^{2+} concentration increases with the Ca^{2+} influxes through VGCCs, and extracellular Ca^{2+} concentration decreases accordingly during the irradiation. Due to the far larger amount of Ca^{2+} ions in extracellular medium compared with those in intracellular medium, the decrement of extracellular Ca^{2+} concentration is insignificant as can be seen from the scales of the concentration in Fig. 7. That is in line with the literature [36]. After the exposure, intracellular Ca^{2+} concentration no longer increases because of the closing of VGCCs.

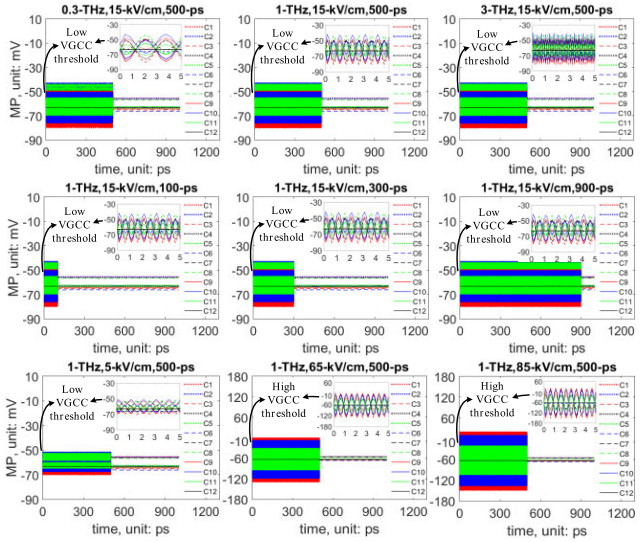

FIGURE 8. MPs at VGCCs C1, C2, ..., C12 with respect to time within 1ns under irradiation of THz electromagnetic waves with different frequencies, electric intensities and irradiation durations. The inset in each figure zooms in on time to show representative vibrations of MPs under each irradiation condition. The thresholds for the activations of low VGCCs −50 mV and high VGCCs −10mV are marked in the figures. At 5-kV/cm electric intensity, MPs at VGCCs are below the threshold. At 15-kV/cm intensity, MPs at C1, C2, C3, C7, C8, C9 and C10 exceed the threshold −50mV. At 65-kV/cm, MPs at C1, C5, C7 and C11 exceed the threshold −50mV, and MPs at C2, C3, C4, C8, C9 and C10 exceed the threshold −10mV. And at 85-kV/cm, MPs at C1, C5, C7 and C11 exceed −50mV, and MPs at C2, C3, C4, C8, C9 and C10 exceed −10mV.

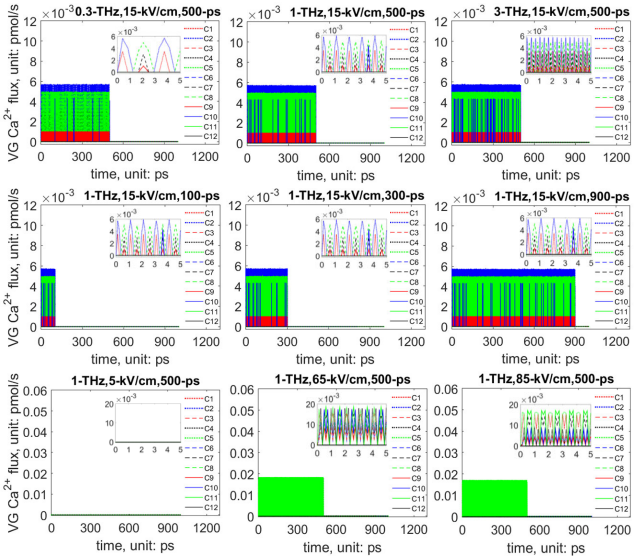

FIGURE 9. VG Ca^{2+} fluxes at C1, C2, . . ., C12 with respect to time within 1ns under the irradiation of THz electromagnetic waves with different frequencies, electric intensities and irradiation durations. The inset in each figure zooms in on time to show representative VG Ca^{2+} fluxes under each irradiation condition.

C. EFFECTS OF IRRADIATION FREQUENCY, DURATION AND ELECTRIC INTENSITY OF THz ELECTROMAGNET-IC WAVE

THz electromagnetic waves with different frequencies, electric intensities and irradiation durations are applied. As the frequency of the THz electromagnetic wave increases, the speed of vibration of MP increases accordingly following the vibration of electric field of the wave (see Fig. 8). And the amplitude as well as the time duration of the vibrations of MP stays invariant with increase of irradiation frequency (Fig. 8). Besides, as the irradiation duration of THz electromagnetic wave increases, the time duration of potential vibrations increases. Meanwhile, the amplitude as well as vibration speed of MP keeps invariant. In addition, the amplitude of vibration of MP increases with the raise of field intensity of the THz electromagnetic wave. In the case of 5-kV/cm THz electromagnetic wave, MP stays below the threshold potential −50 mV for the activation of low VGCCs, and VGCCs keep closed. When the electric intensity of the wave increases to 15-kV/cm, MP exceeds the threshold -50 mV during its vibrations and low VGCCs are open. Further raise of intensity to 65- and 85-kV/cm opens high VGCCs because the MP exceeds the threshold potential -10 mV for activation of high VGCCs (Fig. 8). In the meantime, the speed and time duration of the vibration of MP are independent of the raise of electric intensity (Fig. 8).

Fig. 9 illustrates the voltage-gated Ca^{2+} influxes in response to THz waves with different electromagnetic parameters. From the figure, it can be seen that VG influxes become non-zero when membrane potential exceeds the activation threshold during vibrations. Once the threshold for activation of VGCCs is reached, the irradiation frequency, duration, and electric intensity of THz electromagnetic wave independently impact the speed of change in VG Ca^{2+} fluxes, time duration and magnitude of the fluxes respectively (Fig. 9). In the case of 1-THz, 5-kV/cm, 500-ps electromagnetic irradiation, membrane potential keeps below the threshold for VGCC activation (Fig. 8), which results in zero VG Ca^{2+} influx (Fig. 9).

Profiles of temperature rise from initial 297.15 K in the cell region are shown in Fig. 10. From the figure, the temperature increment increases with the raise of irradiation frequency. This is attributed to the increase in electromagnetic energy loss transferred into heat with the raise of THz frequency. Additionally, both longer irradiation duration and higher electric intensity of the THz wave bring more irradiation energy on the medium, causing larger increment of the temperature (Fig. 10). It is clear that maximum temperature rise is less than 0.6 K in response to THz irradiation with different electromagnetic parameters presented in Fig. 10, indicating the non-thermal effects.

Fig. 11 shows that variations of irradiation frequency from 0.1 to 3 THz have few impact on VGCC activation-induced change in intracellular Ca^{2+} concentration. In the case of different frequencies, although the speed of membrane potential vibration increases with the raise of irradiation frequency, the integral area of membrane potential above the threshold for activation of VGCCs with respect to time is almost the same (Fig. 8). Therefore, the integral area of VG Ca^{2+} influxes with time is almost the same in the case of different frequencies

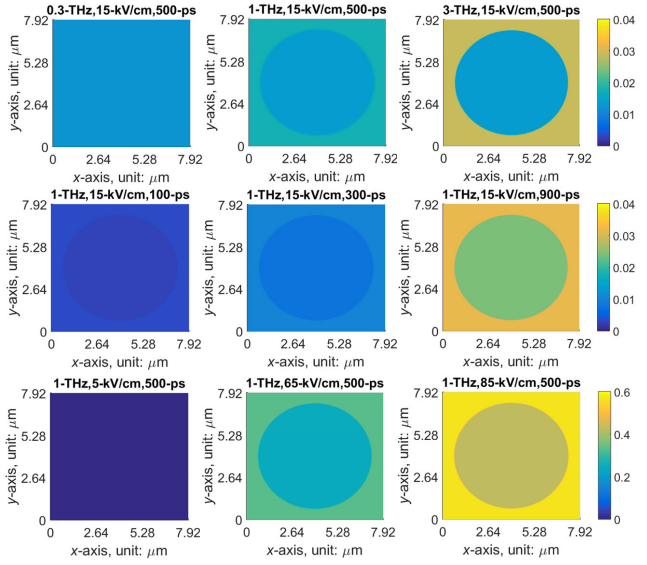

FIGURE 10. Profiles of temperature increments at 1ns in the cell region from initial temperature 297.15 K in response to the irradiation of THz electromagnetic waves with different frequencies, electric intensities and irradiation durations. The values of the temperature rises are presented in K in light of color bars on the right side.

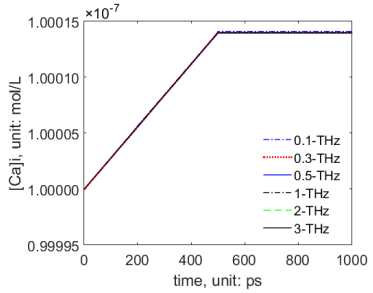

FIGURE 11. Effect of THz electromagnetic frequency on the change in intracellular Ca^{2+} concentration due to VG Ca^{2+} influxes. The irradiated electric intensity and duration are respectively 15-kV/cm and 500-ps.

(Fig. 9), which leads to nearly the same amount of accumulated Ca^{2+} ions within the cell (Fig. 11).

As the irradiation duration of THz electromagnetic wave increases from 100 to 900 ps, increment of intracellular Ca^{2+} concentration increases linearly (Fig. 12). This is as a result of linear increase in the time duration for VG Ca^{2+} influxes with the raise of irradiation duration (Fig. 9).

Fig. 13 and 14 reveal strong nonlinear relation of the concentration increment of intracellular Ca^{2+} ions with respect to electric intensity of irradiated THz electromagnetic wave. Since THz electromagnetic wave of 5-kV/cm electric intensity is incapable of activating VG Ca^{2+} influx (Fig. 8 and 9), intracellular Ca^{2+} concentration does not increase due to VGCCs (Fig. 13 and 14). As the electric intensity increases from 5 to 45 kV/cm so that MP is above the threshold -50 mV during the vibration, low VGCCs are activated (Fig. 8). The activation of VGCCs provides pathways for Ca^{2+} ions to go through between intracellular and extracellular media. There is a huge concentration gradient of Ca^{2+} ions across

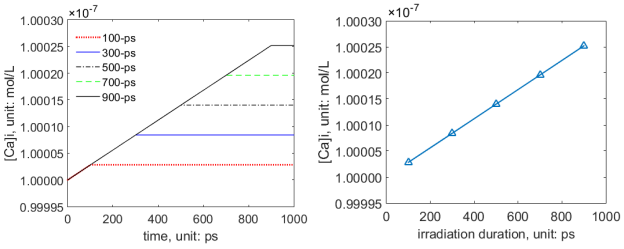

FIGURE 12. Effect of irradiation duration on the change in intracellular Ca^{2+} concentration as a result of VG Ca^{2+} influxes. The irradiated electromagnetic frequency and electric intensity are 1-THz and 15-kV/cm, respectively. The left figure shows the variation of the concentration with time, and the right figure illustrates the concentration collected at 1000ps in the left figure with respect to irradiation duration.

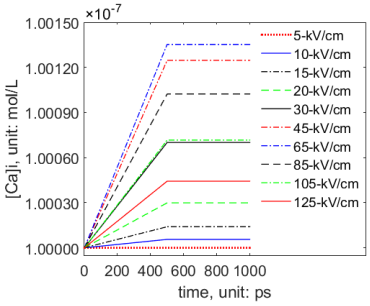

FIGURE 13. Effect of electric intensity on the change in intracellular Ca^{2+} concentration as a result of VG Ca^{2+} influxes. The irradiated electromagnetic frequency and duration are 1-THz and 500-ps, respectively.

the plasma membrane because Ca^{2+} concentration is 1.5mM in extracellular medium and 0.1μM in cytoplasm. Besides, although it increases towards the positive direction, MP is still negative and produces an electric force driving Ca^{2+} into the cell. Therefore, the diffusion force due to the concentration gradient together with the electric force from MP, that is, electrochemical force, drives Ca^{2+} influxes through VGCCs (Fig. 9). The larger the MP is able to reach, the more the VGCCs open, causing larger increment of intracellular Ca^{2+} concentration (Fig. 13 and 14).

When electric intensity increases to 65-kV/cm, MP starts to exceed the threshold -10 mV [29], [30] and high VGCCs are activated besides the low VGCCs (Fig. 8). Activation of high VGCCs produces more Ca^{2+} influxes (Fig. 9) and results in a larger increment of intracellular Ca^{2+} concentration compared with the cases when only low VGCCs are activated (Fig. 13 and 14). However, further increasing the intensity to 85-kV/cm leads to a reduction in the concentration increment (Fig. 13 and 14). As is shown in Fig. 8, MP reaches more positive values in the case of 85-kV/cm compared with 65-kV/cm. In particular, MP can start to be above 0mV in the case of 85-kV/cm (Fig. 8), and the positive MP results in a reverse electric force driving Ca^{2+} fluxes against the concentration gradient. In this case, the electrochemical driving force that drives extracellular Ca^{2+} ions into cell significantly decreases (Fig. 9), although both low and high VGCCs are open for Ca^{2+} ions to go through (Fig. 8). Therefore, the concentration

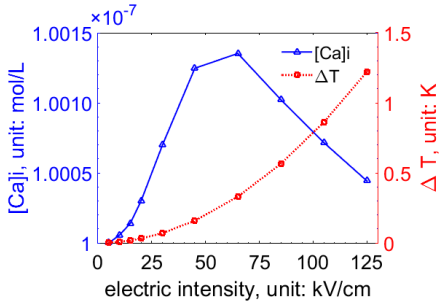

FIGURE 14. Intracellular Ca^{2+} concentration [Ca]i and maximum temperature rise ΔT in the cell region with respect to electric intensity of THz electromagnetic wave. The irradiated electromagnetic frequency and duration are 1 THz and 500 ps, respectively.

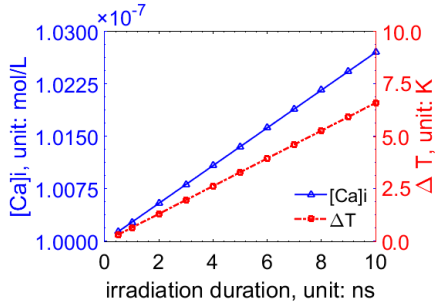

FIGURE 15. Intracellular Ca^{2+} concentration [Ca]i and maximum temperature rise ΔT in the cell region with respect to irradiation duration of THz electromagnetic wave. The irradiated electromagnetic frequency and electric intensity are 1-THz and 65-kV/cm, respectively.

increment decreases as the electric intensity is raised from 65 to 85 kV/cm. Further increasing electric intensity to 105 and 125 kV/cm leads to more reduction of electrochemical driving force on Ca^{2+} ions, and thus more reduction of increment of intracellular Ca^{2+} concentration (Fig. 13 and 14).

Fig. 14 also shows that the THz-induced temperature rise is smaller than 1.22 K although the electric intensity is raised to as large as 125-kV/cm. That indicates the non-thermal bioeffects of the applied THz electromagnetic irradiations.

D. HIGH-DOSE TERAHERTZ IRRADIATION

Temperature rise along with increment of intracellular Ca^{2+} concentration in response to high-dose THz irradiation is studied by raising irradiation duration to nanosecond. Fig. 15 illustrates the increments of temperature and intracellular Ca^{2+} concentration as the irradiation duration of 1-THz, 65-kV/cm electromagnetic wave increases from 500 ps to 10 ns. As longer irradiation duration induces longer activation of VGCCs, increment of intracellular Ca^{2+} concentration increases accordingly (Fig. 15). In addition, raising irradiation duration from 500 ps to 10 ns results in the temperature rise from 0.33 to 6.60 K (Fig. 15), because longer irradiation duration brings more electromagnetic energy losses transferred into heat on the medium. As the temperature increment keeps rising with the increase in irradiation duration, the thermal bioeffects of the THz electromagnetic irradiation begin to become more and more pronounced.

V. CONCLUSION

According to the electromagnetic analyses on the basis of relativistic electrodynamics at the cellular level, the electromagnetic interaction between 0.1 ∼ 3 THz electromagnetic fields and mobile physiological ions in the cell region is primarily electric interaction, and magnetic interaction is negligible.

And from numerical simulations, membrane potential vibrates with the vibration of electric field in terahertz electromagnetic wave. Voltage-gated Ca^{2+} channels are activated when membrane potential exceeds the threshold potential for activation of voltage-gated Ca^{2+} channels during its vibration. The activation of VGCCs induces VG Ca^{2+} influx from extracellular medium and raises intracellular Ca^{2+} concentration accordingly. In the meantime, change in membrane potential and variations of intracellular Ca^{2+} concentration trigger the active transport mechanism in plasma membrane to pump Ca^{2+} out. However, the active transport Ca^{2+} effluxes are six orders of magnitude smaller than VG Ca^{2+} influxes during the THz irradiation, which makes active transport of Ca^{2+} ions negligible in this process.

In addition, the numerical results reveal the relation of the increment of intracellular Ca^{2+} concentration resulting from activation of VGCCs to terahertz electromagnetic parameters. Raising irradiation duration from 100 to 900ps significantly increases the increment of intracellular Ca^{2+} concentration linearly. In contrast, varying electromagnetic frequency from 0.1 to 3THz has little influence on the concentration increment. As for electric intensity of the terahertz electromagnetic wave, it shows a strong nonlinear relationship with the concentration increment. In the case of 5-kV/cm electric intensity, VGCCs stay closed and are incapable of causing increase in intracellular Ca^{2+} concentration. In the case of electric intensity from 10 to 45 kV/cm, activation of low VGCCs induces Ca^{2+} influxes from extracellular medium and hence intracellular Ca^{2+} concentration increases. When the electric intensity is 65 kV/cm, high VGCCs are open and produce a larger concentration increment in comparison with 45-kV/cm electric intensity. Further increase in electric intensity from 65 to 125 kV/cm results in reduction of the concentration increment as a consequence of the reduction of electrochemical driving force on Ca^{2+} ions in spite of the activation of both low and high VGCCs. In the meantime, numerical results show that the THz-induced temperature rises are insignificant under the irradiation conditions above in the study with different electromagnetic parameters, indicating the non-thermal bioeffects.

Furthermore, numerical simulation also reveals that thermal effects can be pronounced as long as the irradiation duration is raised to be long enough for high-dose irradiation of terahertz electromagnetic wave.

Those conclusions provide a pioneering understanding of the bioeffect of terahertz irradiation on Ca^{2+} transmembrane transport through voltage-gated Ca^{2+} channels, and lay the foundation for further research in modulation of intracellular Ca^{2+} concentration with terahertz electromagnetic waves.

REFERENCES

[1] P. Siegel, "Terahertz technology in biology and medicine," *IEEE Trans. Microw. Theory Techn.*, vol. 52, no. 10, pp. 2438–2447, Oct. 2004.
[2] S. Fan, Y. He, B. S. Ung, and E. Pickwell-MacPherson, "The growth of biomedical terahertz research," *J. Phys. D, Appl. Phys.*, vol. 47, no. 37, Sep. 2014, Art. no. 374009.
[3] R. Zhou, C. Wang, W. Xu, and L. Xie, "Biological applications of terahertz technology based on nanomaterials and nanostructures," *Nanoscale*, vol. 11, no. 8, pp. 3445–3457, Jan. 2019.
[4] F. Wang, D. Zhao, L. Jiang, J. Song, and Y. Liu, "THz vibrational spectroscopy for RNA basepair cocrystals and oligonucleotide sequences," *Spectrochimica Acta A, Molecular Biomol. Spectrosc.*, vol. 209, pp. 49–54, Feb. 2019.
[5] B. C. Q. Truong, H. D. Tuan, V. P. Wallace, A. J. Fitzgerald, and H. T. Nguyen, "The potential of the double debye parameters to discriminate between basal cell carcinoma and normal skin," *IEEE Trans. THz Sci. Technol.*, vol. 5, no. 6, pp. 990–998, Nov. 2015.
[6] G. J. Wilmink and J. E. Grundt, "Invited review article: Current state of research on biological effects of terahertz radiation," *J. Infr., Millim., THz. Waves*, vol. 32, no. 10, pp. 1074–1122, Oct. 2011.
[7] A. R. Orlando and G. P. Gallerano, "Terahertz radiation effects and biological applications," *J. Infr., Millim., THz. Waves*, vol. 30, pp. 1308–1318, Dec. 2009.
[8] D. R. Dalzell, J. McQuade, R. Vincelette, B. Ibey, J. Payne, and R. Thomas, *Damage Thresholds for Terahertz Radiation*, vol. 7562. Bellingham, WA, USA: SPIE, 2010.
[9] G. J. Wilmink, B. D. Rivest, B. L. Ibey, C. L. Roth, J. Bernhard, and W. P. Roach, *Quantitative Investigation of the Bioeffects Associated With Terahertz Radiation*, vol. 7562. Bellingham, WA, USA: SPIE, 2010.
[10] W. Bo, J. Tang, Y. Yang, J. Ma, Q. Huang, L. Guo, Z. Wang, Z. Wu, B. Zeng, and Y. Gong, "A numerical study for dielectric constant profile of aqueous solvent in ionic solution radiated by high-intensity electric pulses," *AIP Adv.*, vol. 8, no. 11, Nov. 2018, Art. no. 115217.
[11] J. R. Peacock, "Millimetre wave permittivity of water near 25°C," *J. Phys. D, Appl. Phys.*, vol. 42, no. 20, Oct. 2009, Art. no. 205501.
[12] G. J. Wilmink, B. D. Rivest, C. C. Roth, B. L. Ibey, J. A. Payne, L. X. Cundin, J. E. Grundt, X. Peralta, D. G. Mixon, and W. P. Roach, "*In vitro* investigation of the biological effects associated with human dermal fibroblasts exposed to 2.52 THz radiation," *Lasers Surg. Med.*, vol. 43, no. 2, pp. 152–163, Feb. 2011.
[13] N. Ostrovskiy, C. Nikituk, V. Kirichuk, A. Krenitskiy, A. Majborodin, V. Tupikin, and G. Shub, "Application of the Terahertz Waves in Therapy of Burn Wounds," in *Proc. Joint 30th Int. Conf. Infr. Millim. Waves 13th Int. Conf. THz. Electron.*, Williamsburg, VA, USA, Jan. 2006, pp. 301–302.
[14] V. F. Kirichuck, A. N. Ivanov, O. N. Antipova, A. P. Krenickiy, A. V. Mayborodin, and V. D. Tupikin, "Sex-specific differences in changes of disturbed functional activity of platelets in albino rats under the effect of Terahertz electromagnetic radiation at nitric oxide frequencies," *Bull. Exp. Biol. Med.*, vol. 145, no. 1, pp. 75–77, Jan. 2008.
[15] V. F. Kirichuk, E. V. Andronov, N. V. Mamontova, V. D. Tupicin, and A. V. Mayborodin, "Use of Terahertz electromagnetic radiation for correction of blood rheology parameters in patients with unstable angina under conditions of treatment with isoket, an NO donor," *Bull. Exp. Biol. Med.*, vol. 146, no. 3, pp. 293–296, Sep. 2008.
[16] V. F. Kirichuk, N. V. Efimova, and E. V. Andronov, "Effect of high power Terahertz irradiation on platelet aggregation and behavioral reactions of albino rats," *Bull. Exp. Biol. Med.*, vol. 148, no. 5, pp. 746–749, Nov. 2009.
[17] P. T. Vernier, Z. A. Levine, M.-C. Ho, S. Xiao, I. Semenov, and A. G. Pakhomov, "Picosecond and Terahertz perturbation of interfacial water and electropermeabilization of biological membranes," *J. Membrane Biol.*, vol. 248, no. 5, pp. 837–847, Oct. 2015.
[18] A. G. Pakhomov, S. Grigoryev, I. Semenov, M. Casciola, C. Jiang, and S. Xiao, "The second phase of bipolar, nanosecond-range electric pulses determines the electroporation efficiency," *Bioelectrochemistry*, vol. 122, pp. 123–133, Aug. 2018.
[19] W. Bo, J. Tang, J. Ma, and Y. Gong, "Numerical study on calcium transport through voltage-gated calcium channels in response to nanosecond pulsed electric field," *IEEE Trans. Plasma Sci.*, vol. 46, no. 7, pp. 2562–2572, Jul. 2018.
[20] E. C. Gianulis, M. Casciola, S. Xiao, O. N. Pakhomova, and A. G. Pakhomov, "Electropermeabilization by uni-or bipolar nanosecond electric pulses: The impact of extracellular conductivity," *Bioelectrochemistry*, vol. 119, pp. 10–19, Feb. 2018.
[21] J. Tang, H. Yin, J. Ma, W. Bo, Y. Yang, J. Xu, Y. Liu, and Y. Gong, "Terahertz electric field-induced membrane electroporation by molecular dynamics simulations," *J. Membrane Biol.*, vol. 251, nos. 5–6, pp. 681–693, Dec. 2018.
[22] W. Bo, J. Xu, J. Tang, Y. Yang, J. Ma, Z. Wang, and Y. Gong, "Numerical simulation on voltage-activated calcium flux of neuroblastoma cells in response to 2.5 THz electric pulses," in *Proc. 42nd Int. Conf. Infr., Millim., THz. Waves (IRMMW-THz)*, Aug. 2017, pp. 1–2.
[23] G. J. Wilmink, B. L. Ibey, C. L. Roth, R. L. Vincelette, B. D. Rivest, and C. B. Horn, *Determination of Death Thresholds and Identification of Terahertz (THz)-Specific Gene Expression Signatures*, vol. 7562. Bellingham, WA, USA: SPIE, 2010.
[24] C. B. Reid, G. Reese, A. P. Gibson, and V. P. Wallace, "Terahertz time-domain spectroscopy of human blood," *IEEE Trans. THz Sci. Technol.*, vol. 3, no. 4, pp. 363–367, Jul. 2013.
[25] M. L. T. Asaki, A. Redondo, T. A. Zawodzinski, and A. J. Taylor, "Dielectric relaxation of electrolyte solutions using Terahertz transmission spectroscopy," *J. Chem. Phys.*, vol. 116, no. 19, p. 8469, 2002.
[26] R. F. Harrington, *Time-Harmonic Electromagnetic Fields*. Piscataway, NJ, USA: IEEE Press, 2001, pp. 9–12.
[27] R. Joshi, Q. Hu, and K. Schoenbach, "Modeling studies of cell response to ultrashort, high-intensity electric fields-implications for intracellular manipulation," *IEEE Trans. Plasma Sci.*, vol. 32, no. 4, pp. 1677–1686, Aug. 2004.
[28] H. Lodish, A. Berk, P. Matsudaira, C. A. Kaiser, M. Krieger, and M. P. Scott, *Molecular Cell Biology*, 5th ed. San Francisco, CA, USA: Freeman, 2003, pp. 245–251.
[29] R. J. Docherty, "Gadolinium selectively blocks a component of calcium current in rodent neuroblastoma x glioma hybrid (NG108-15) cells," *J. Physiol.*, vol. 398, no. 1, pp. 33–47, Apr. 1988.
[30] D. A. Brown and H. Higashida, "Membrane current responses of 9 mouse neuroblastoma x rat glioma hybrid cells to bradykinin," *J. Physiol.*, vol. 397, pp. 84–167, Mar. 1988.
[31] A. V. Melkikh and V. D. Seleznev, "Models of active transport of ions in biomembranes of various types of cells," *J. Theor. Biol.*, vol. 234, no. 3, pp. 403–412, Jun. 2005.
[32] K. Kurzinger, C. Stadtkus, and B. Hamprecht, "Uptake and energy-dependent extrusion of calcium in neural cells in culture," *Eur. J. Biochem.*, vol. 103, no. 3, pp. 597–611, Feb. 1980.
[33] J. Li, W. Tan, M. Yu, and H. Lin, "The effect of extracellular conductivity on electroporation-mediated molecular delivery," *Biochimica et Biophysica Acta (BBA)-Biomembranes*, vol. 1828, no. 2, pp. 461–470, Feb. 2013.
[34] B. Corry, T. W. Allen, S. Kuyucak, and S.-H. Chung, "A model of calcium channels," *Biochimica et Biophysica Acta (BBA)-Biomembranes*, vol. 1509, pp. 1–6, Dec. 2000.
[35] B. Corry, T. W. Allen, S. Kuyucak, and S.-H. Chung, "Mechanisms of permeation and selectivity in calcium channels," *Biophys. J.*, vol. 80, no. 1, pp. 195–214, Jan. 2001.
[36] J. Malmivuo and R. Plonsey, *Bioelectromagnetism: Principles and Applications of Bioelectric and Biomagnetic Fields*. New York, NY, USA: Oxford Univ. Press, 1995, pp. 45–56.

WENFEI BO was born in Xinzhou, Shanxi, China, in 1992. He received the B.S. degree from the University of Electronic Science and Technology of China (UESTC), Chengdu, China, in 2014, where he is currently pursuing the Ph.D. degree in physical electronics. From 2018 to 2019, he studied in Frank Reidy Research Center for Bioelectrics in Old Dominion University. His current research interests mainly include bioeffects of nanosecond pulsed electric fields, and terahertz electromagnetic fields on ion transport and the application.

LIANGHAO GUO was born in Yantai, Shandong, China, in 1995. He received the B.E. degree from Dalian Maritime University (DLMU), Dalian, China, in 2017. He is currently pursuing the Ph.D. degree in electronic science and technology with the University of Electronic Science and Technology of China (UESTC), Chengdu, China.

His current research interest mainly includes terahertz biological effects at the single-cell level.

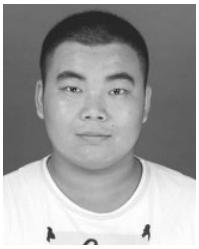

YANG YANG received the B.S. degree in vacuum electronics from the University of Electronic Science and Technology of China, Chengdu, China, in 2015, where he is currently pursuing the Ph.D. degree in physical electronics with the National Key Laboratory of Science and Technology on Vacuum Electronics. His research interests include water-immersed antenna, OAM antenna, and microwave imaging.

JIALU MA was born in Yuzhou, Henan, China, in 1991. He is currently pursuing the Ph.D. degree in electronic science and technology with the University of Electronic Science and Technology of China (UESTC), Chengdu, China.

KAICHENG WANG was born in Fuqing, Fujian, China, in 1995. He received the B.S. degree from the University of Electronic Science and Technology of China (UESTC), Chengdu, China, in 2018, where he is currently pursuing the Ph.D. degree in electronic science and technology.

His researches focus on terahertz biophysics and terahertz intense field biochemical effects.

JINGCHAO TANG was born in Qingdao, Shandong, China, in June 1991. He is currently pursuing the Ph.D. degree in electronic science and technology with the University of Electronic Science and Technology of China (UESTC), Chengdu, China.

His current research interest mainly includes biophysics.

ZHE WU received the Ph.D. degree in physics, in 2008. From 2012 to 2014, she was a Research Fellow with the National University of Singapore. She is currently an Associate Professor with the School of Physics, University of Electronic Science and Technology of China. Her research interests include electromagnetic parametric measurements, electromagnetic field simulation, and application for microwave energy.

BAOQING ZENG received the Ph.D. degree in physical electronics from the University of Electronic Science and Technology of China, Chengdu, China, in 1999.

He has been with the National Key Laboratory of Science and Technology on Vacuum Electronics, School of Physical Electronics, UESTC, since 1999. He has authored and coauthored more than 100 research articles. His research interests include field emission, nanomaterials synthesis and application, and microwave power applications.

YUBIN GONG (Member, IEEE) was born in Yantai, Shandong, China, in 1967. He received the B.S. degree from the Changchun University of Science and Technology, Changchun, China, in 1989, and the M.S. and Ph.D. degree in physical electronics from the University of Electronic Science and Technology of China (UESTC), Chengdu, China, in 1992 and 1998, respectively.

He is currently a Professor with UESTC. He has authored or coauthored over 200 research articles. His current research interests include bioeffects of pulsed electric fields and electromagnetic fields radiation and the application, biomedical imaging, and broadband high-power traveling-wave tubes.